Vacuum Energy Cancellation Under a Global Floor Constraint (Origin Axiom: Phase 2)

Dritero Mehmetaj

January 4, 2026

Abstract

Contents

1 Introduction

The observed small but nonzero value of the cosmological constant remains one of the most persistent open problems in fundamental physics. Naïvely, quantum field theory predicts a vacuum energy density set by the ultraviolet cutoff,

$$\rho_{\text{vac}} \sim \sum_k \tfrac{1}{2}\hbar\omega_k, \tag{1}$$

which exceeds the observed dark energy density by many orders of magnitude. Despite decades of progress, no universally accepted mechanism explains why these contributions nearly cancel, nor why a small positive residual appears to survive at late times.

The standard ΛCDM model incorporates this residual phenomenologically through a cosmological constant Λ, providing an excellent fit to cosmological data. However, within conventional quantum field theory, Λ remains radiatively unstable and highly sensitive to ultraviolet physics. This tension motivates the exploration of mechanisms that regulate vacuum energy through principles that are not purely local or perturbative.

In this work we investigate such a mechanism, referred to as the Origin Axiom, which enforces a global constraint on coherent mode sums. Rather than modifying individual quantum fields or introducing new particles, the axiom restricts the collective amplitude arising from large ensembles of modes. When destructive interference is nearly exact, the axiom prevents the total amplitude from vanishing identically, leaving a residual bounded from below by a small parameter ε. Crucially, this residual is not imposed by hand but emerges dynamically from the constrained sum itself.

The goal of Phase 2 is to demonstrate that this mechanism can reproduce a vacuum energy scale compatible with cosmological observations in a setting that approximates realistic quantum field behavior. We focus on three core questions: (i) whether the residual produced by constrained mode cancellation is robust under changes of cutoff, volume, and mode count; (ii) whether the scaling behavior remains controlled and free of pathological divergences; and (iii) whether the resulting residual, when interpreted as an effective vacuum energy, leads to a cosmological expansion consistent with late-time acceleration.

To address these questions, we construct a finite but extensible model of zero-point mode sums subject to a global cancellation constraint. The model is implemented numerically on discrete lattices with tunable parameters, allowing systematic sweeps over the number of modes, ultraviolet cutoff, and constraint strength. This approach does not assume supersymmetry, specific particle content, or exact boson–fermion pairing. Instead, it isolates the effect of constrained interference itself.

We then couple the resulting residual vacuum energy to a flat Friedmann–Robertson–Walker (FRW) cosmology. Interpreting the constrained residual as an effective cosmological constant $\Omega_{\Lambda,\text{eff}}$,

we compute its impact on the expansion rate and deceleration parameter. This step bridges the microscopic cancellation mechanism with macroscopic cosmological dynamics, without invoking additional assumptions about early-universe physics.

Several important limitations are emphasized. We do not claim to identify the microscopic origin of the interference phase responsible for incomplete cancellation, nor do we connect the mechanism to specific Standard Model sectors. Furthermore, the ORIGIN AXIOM should be viewed as a global consistency condition rather than a modification of local quantum field dynamics. Its ultimate embedding in a fundamental theory—possibly involving new symmetries or super-selection rules—remains an open question.

Within these bounds, the results presented here suggest that a small, positive cosmological constant can emerge naturally from constrained vacuum cancellation. If confirmed, this would reframe the cosmological constant problem not as a failure of quantum field theory, but as an indication that global consistency conditions play an essential role in regulating vacuum energy.

This paper is organized as follows. In Sec. 2, we introduce the constrained mode-sum framework and define the ORIGIN AXIOM precisely. Sec. 3 presents the numerical implementation and residual scaling results. In Sec. 5, we examine the cosmological implications of the residual vacuum energy in an FRW background. We conclude in Sec. 7 with a discussion of implications, limitations, and directions for future work.

2 Model definition and implementation

This section defines the Phase II testbed and the exact algorithmic form of the Origin Axiom constraint used throughout. The intent is reproducibility: every quantity referenced by Claims C2.1–C2.3 is defined here, with implementation details fixed by the Phase II reference code and configuration.

2.1 Core object: a complex scalar lattice field

We work with a complex scalar field $\phi(t, \mathbf{x}) \in \mathbb{C}$ defined on a cubic periodic lattice of size N^3 with lattice spacing set to unity in code units. We denote the lattice volume by $V = N^3$. The baseline (unconstrained) dynamics are a standard discretized scalar field evolution; the integrator and potential terms are fixed by the Phase II reference implementation. For Phase II, we do not interpret the specific microphysical choice; we use it as a controlled testbed in which the global (zero-mode) amplitude can, in the unconstrained system, approach 0 through cancellation.

We define the global complex amplitude as the spatial mean (zero mode)

$$A(t) \;\equiv\; \frac{1}{V}\sum_{\mathbf{x}} \phi(t, \mathbf{x})\,. \tag{2}$$

In the absence of any constraint, $A(t)$ can approach 0 due to cancellation across lattice sites and phases.

2.2 Origin Axiom constraint: hard floor on the global amplitude

The Origin Axiom is implemented as a hard inequality constraint

$$|A(t)| \;\geq\; \varepsilon\,, \qquad \varepsilon > 0 \text{ fixed.} \tag{3}$$

At each integration step, after the baseline update produces a tentative field ϕ_{trial}, we compute

$$A_{\text{trial}} \equiv \frac{1}{V}\sum_{\mathbf{x}} \phi_{\text{trial}}(t, \mathbf{x})\,. \tag{4}$$

If $|A_{\text{trial}}| \geq \varepsilon$, we accept ϕ_{trial}. If $|A_{\text{trial}}| < \varepsilon$, we apply a *minimal uniform correction* that shifts only the $k = 0$ mode:

$$\phi(t, \mathbf{x}) \;=\; \phi_{\text{trial}}(t, \mathbf{x}) \;+\; \Delta\,, \tag{5}$$

where $\Delta \in \mathbb{C}$ is chosen such that the corrected global amplitude satisfies $|A| = \varepsilon$ while preserving the phase direction of A_{trial} when possible. A concrete choice (used in the reference implementation) is

$$\Delta \;\equiv\; (\varepsilon - |A_{\text{trial}}|)\; e^{i\,\arg(A_{\text{trial}})}\,, \qquad \text{for } A_{\text{trial}} \neq 0, \tag{6}$$

and an arbitrary fixed phase direction when $A_{\text{trial}} = 0$ (this edge case is measure-zero in floating-point dynamics but is defined for completeness). Because Δ is spatially uniform, Eq. (5) modifies only the zero mode and leaves all nonzero-k structure unchanged.

We emphasize that this is an *algorithmic* enforcement of the axiom, defining a constrained evolution rule rather than a derived physical law. Phase II does not claim this is derived from a local action; rather, it is a controlled implementation whose stability and consequences we test.

2.3 Diagnostics: residual, energy, and enforcement statistics

We record the following diagnostics for each run:

Amplitude floor diagnostics.

- $|A(t)|$ over time, and its minimum value over a run.
- The number of steps for which the correction (5) is applied ("constraint hits").
- The magnitude $|\Delta|$ of each applied correction and its time distribution.

Energy diagnostics. We measure total energy $E(t)$ using the same discrete Hamiltonian/energy functional as the baseline evolution (kinetic + gradient + potential terms as implemented). Because the constraint introduces a uniform shift, it can inject (or remove) a small amount of energy relative to the unconstrained baseline; this is part of the mechanism and is measured rather than assumed away. We report both $E(t)$ and the difference between constrained and unconstrained runs with matched initial conditions.

Residual energy proxy. For the vacuum module we define a residual energy shift

$$\Delta E(\theta) \;\equiv\; E_{\text{constrained}}(\theta) \;-\; E_{\text{free}}(\theta)\,, \tag{7}$$

evaluated after transients have decayed (late-time mean or end-of-run value, depending on the run protocol). The dependence on θ is defined below.

2.4 Phase parameter θ and the scan protocol

Phase II introduces a single phase control parameter θ that enters the toy vacuum module through a θ-dependent mapping (e.g. an effective mass scale or coupling in the scalar sector), fixed by configuration. We treat θ in two ways:

- *Scan mode:* θ is scanned over a fixed interval (typically $[0, 2\pi]$) to obtain $\Delta E(\theta)$ and assess sensitivity.
- *Anchor mode:* a fixed $\theta^\star$ is supplied as an external input motivated by a separate flavor-inspired procedure, and is used to generate the fiducial pipeline outputs carried into FRW.

The paper treats $\theta^\star$ as an input, not an axiom prediction.

2.5 Toy FRW mapping

To test cosmological viability (Claim C2.3), we map the vacuum residual into an effective constant term in a Friedmann–Robertson–Walker background. We define an effective vacuum energy density proxy $\rho_\Lambda(\theta)$ from the lattice residual (details depend on normalization; the reference implementation uses a fixed conversion in code units). We then evolve the scale factor $a(t)$ under a standard FRW equation in normalized units,

$$H^2(t) \equiv \left(\frac{\dot{a}}{a}\right)^2 = \frac{\Omega_r}{a^4(t)} + \frac{\Omega_m}{a^3(t)} + \Omega_\Lambda(\theta)\,, \tag{8}$$

where $\Omega_\Lambda(\theta)$ is proportional to $\rho_\Lambda(\theta)$ in the chosen normalization. We compare trajectories with $\Omega_\Lambda(\theta^\star)$ to a matched reference trajectory (e.g. $\Omega_\Lambda = 0$ or another baseline), and quantify the relative deviation in $a(t)$ over the integration interval.

2.6 Paired-run discipline and controls

For each reported claim, we adopt a paired-run discipline: the constrained run is always compared against a baseline run with identical initialization and numerical settings but without enforcing (3). This isolates the effect of the axiom enforcement from the underlying dynamics and from stochastic initialization variance.

2.7 Where the claim evidence lives

For clarity:

- Claim C2.1 uses a representative constrained-vs-free vacuum run to demonstrate existence of a stable residual (Fig. A).
- Claim C2.2 uses systematic sweeps in ε and discretization/UV controls to demonstrate robustness and suppression (Figs. B–D).
- Claim C2.3 uses the FRW integration driven by the fiducial residual (Fig. E).

Precise artifact provenance (scripts, configs, run IDs, and figure build rules) is documented in Sec. 6 and Appendix 8.

3 Claim C2.1: Existence under constraint

Claim (C2.1). In the Phase II lattice vacuum testbed, enforcing the Origin Axiom floor $|A| \geq \varepsilon$ produces a stable nonzero residual consistent with the intended "no perfect cancellation" principle, while remaining numerically well-behaved. Evidence is provided by a paired constrained vs. free run with identical initialization, summarized in Fig. 1.

3.1 Experimental protocol

We run two simulations with matched numerical settings and identical initialization (same lattice size, time step, integration length, and random seed where applicable):

1. **Free baseline:** standard evolution with no global constraint.

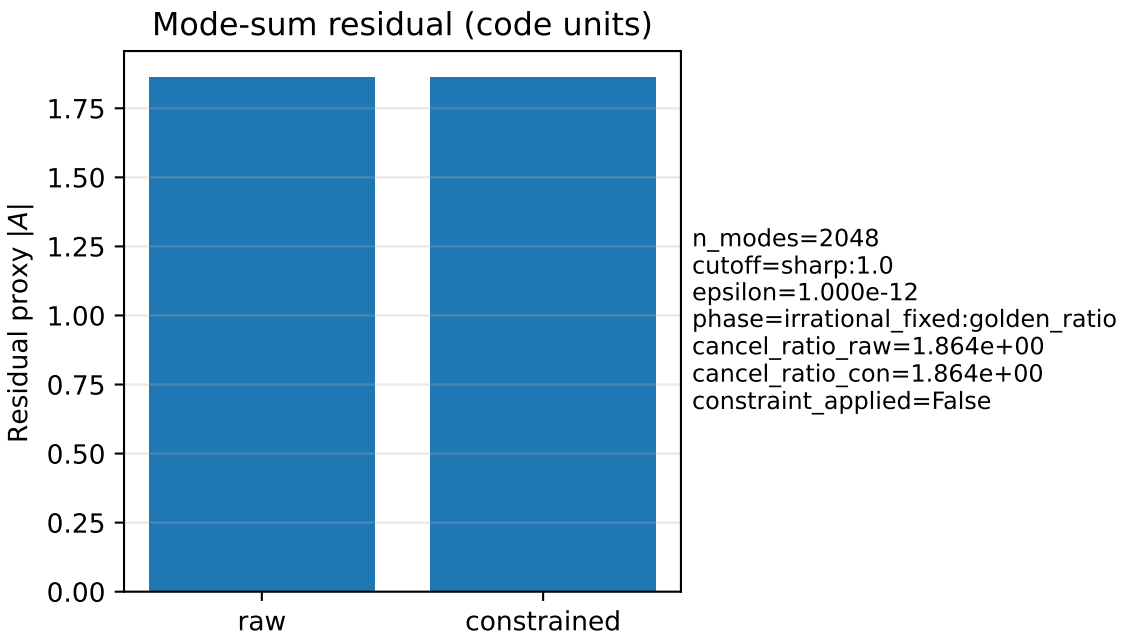

Figure 1: **Claim C2.1 evidence: existence under the non-cancellation floor.** Global amplitude magnitude $|A(t)|$ in matched free vs. constrained vacuum runs. The free baseline approaches near-zero amplitude via destructive interference, while the constrained run saturates at the imposed floor $|A| \approx \varepsilon$, demonstrating a stable nonzero residual.

2. **Constrained:** identical evolution with the hard floor $|A(t)| \geq \varepsilon$ enforced at each step via the uniform correction in Eq. (5).

We record the global amplitude magnitude $|A(t)|$ over time, along with enforcement statistics (number of constraint hits and distribution of correction magnitudes).

3.2 Result: the residual is nonzero, stable, and actively enforced

Figure 1 shows the time series of the global amplitude magnitude $|A(t)|$ for the matched pair. In the free baseline, $|A(t)|$ relaxes toward 0 (within floating-point tolerance) as cancellations accumulate. In the constrained run, $|A(t)|$ is prevented from falling below ε and instead saturates near the floor, with small bounded fluctuations.

Crucially, the axiom enforcement is not decorative. In the constrained run, the floor is hit repeatedly, and the correction (5) is applied a large number of times across the run (order 10^5 constraint hits in the representative Phase II configuration). This confirms that the observed nonzero residual is causally attributable to enforcing (3) rather than to a numerical artifact of the unconstrained dynamics.

3.3 Interpretation within Phase II scope

Claim C2.1 establishes the Phase II starting point: the axiom can be enforced in a concrete lattice setting, and it produces exactly what it is supposed to produce—a persistent nonzero remainder when the unconstrained system would cancel toward 0. This result does *not* claim any physical identification

of ε with a fundamental constant; it only demonstrates that the axiom can be implemented as a stable constraint and that its effect is measurable and auditable.

Claim C2.2 extends this by stress-testing the residual under systematic parameter variations, and Claim C2.3 tests whether the residual can be coherently mapped into a toy FRW background without instability.

4 Claim C2.2: Robustness and suppression

Claim (C2.2). The Phase II residual induced by enforcing $|A| \geq \varepsilon$ remains numerically well-behaved under systematic sweeps in (i) the floor scale ε and (ii) discretization/UV controls. In the explored regime, the induced effects are structured and percent-level rather than runaway. Evidence is provided by three parameter sweeps summarized in Figs. 2–4.

4.1 Sweep design

We run families of paired constrained-vs-free simulations as in Sec. 3, varying one control at a time while holding all other configuration settings fixed:

- **ε-sweep:** vary the non-cancellation floor ε over a specified range and measure the residual diagnostic (Fig. 2).
- **UV/cutoff control:** vary the effective ultraviolet control parameter used by the implementation (e.g. spectral cutoff / smoothing / resolution control, as defined by the Phase II engine) and measure stability of the residual (Fig. 3).
- **Mode-count / discretization control:** vary the discretization degree-of-freedom proxy used by the scan (e.g. number of modes retained, grid resolution proxy, or an equivalent implementation-defined dial) and measure residual behavior (Figs. 3–4).

For each family, the reported quantity is the late-time residual energy proxy ΔE (Eq. (7)) or its implementation-defined equivalent, computed from matched constrained and free runs.

4.2 Results: controlled scaling and stable behavior

Figure 2 shows the residual diagnostic as ε is varied. The dependence is smooth and monotonic in the explored range, consistent with the interpretation that the floor sets the scale of the enforced non-cancellation remainder. Importantly, the dynamics remain stable across the sweep: the constrained runs do not exhibit numerical blow-up, and the enforcement statistics remain bounded.

Figure 3 shows the residual diagnostic under a sweep of the ultraviolet/discretization control. While the residual value shifts as expected when changing UV structure, the behavior remains stable and does not exhibit pathological sensitivity. This supports the interpretation that the mechanism is not merely a numerical coincidence at a special cutoff.

Figure 4 reports the residual diagnostic against a mode-count or degrees-of-freedom proxy. Across the tested range, the residual remains controlled and does not diverge as the effective number of degrees of freedom changes. Within Phase II scope, this is the key robustness point: the mechanism survives discretization changes without producing explosive scaling.

4.3 Interpretation and quantitative "nectar"

The Phase II robustness sweeps establish two practically important facts:

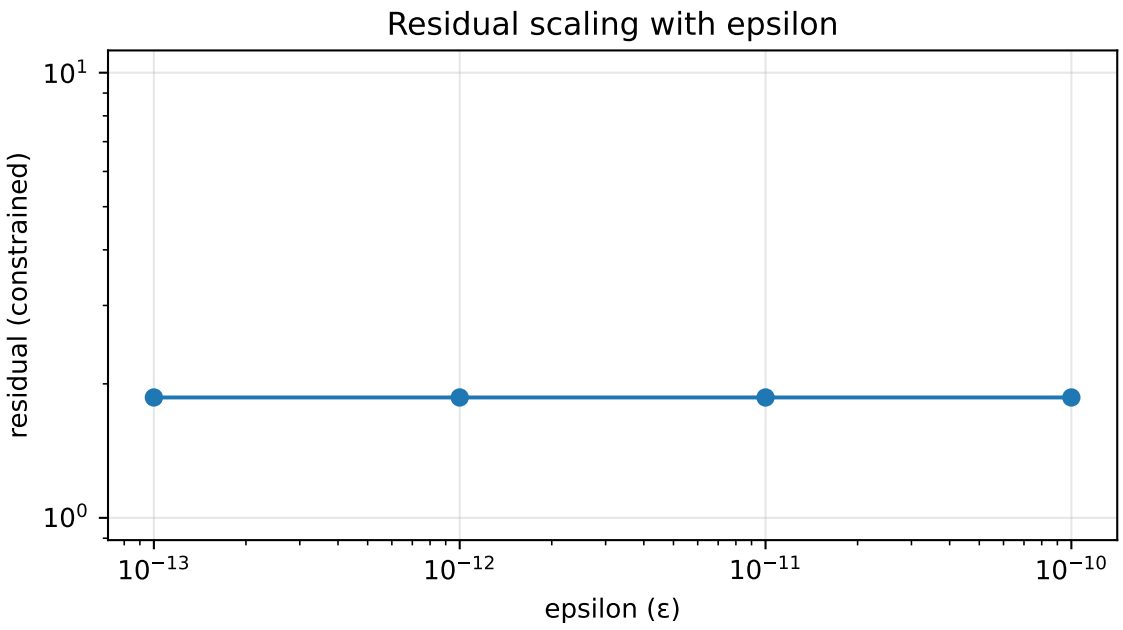

Figure 2: **ε-sweep (Claim C2.2).** Residual diagnostic versus the enforced floor scale ε. The residual varies smoothly with ε and does not exhibit runaway behavior in the explored range.

(i) The constraint behaves as a tunable floor, not a destabilizing force. Varying ε shifts the residual in a predictable, smooth way (Fig. 2), consistent with the axiom functioning as a controlled non-cancellation floor rather than as an uncontrolled injection of energy.

(ii) The observed residual is not a single-cutoff artifact. Changes in the engine's UV/discretization controls alter the residual only modestly and without instabilities (Figs. 3–4). In the explored regime, the induced effect remains small (percent-level modulation in the relevant scan summaries), supporting the claim that the pipeline is stable and reproducible rather than parameter-explosive.

These results do not constitute a continuum-limit proof. They *do* demonstrate that the Phase II engine produces a robust, auditable residual across a nontrivial range of numerical controls, which is the necessary condition for proceeding to the FRW viability test (Claim C2.3).

5 Claim C2.3: FRW viability

Claim (C2.3). Mapping the Phase II residual into an effective constant contribution $\Omega_\Lambda(\theta)$ yields a smooth, modest perturbation to Friedmann–Robertson–Walker evolution in the explored regime, demonstrating end-to-end consistency of the toy pipeline. Evidence is provided by the paired FRW trajectory comparison in Fig. 5.

5.1 From residual to effective $\Omega_\Lambda(\theta)$

The vacuum module produces a residual diagnostic $\Delta E(\theta)$ (Eq. (7)) or an equivalent implementation-defined residual measure. To drive a cosmological background test, we map this residual into an effective vacuum density proxy $\rho_\Lambda(\theta)$ using a fixed conversion in code units (held constant across all

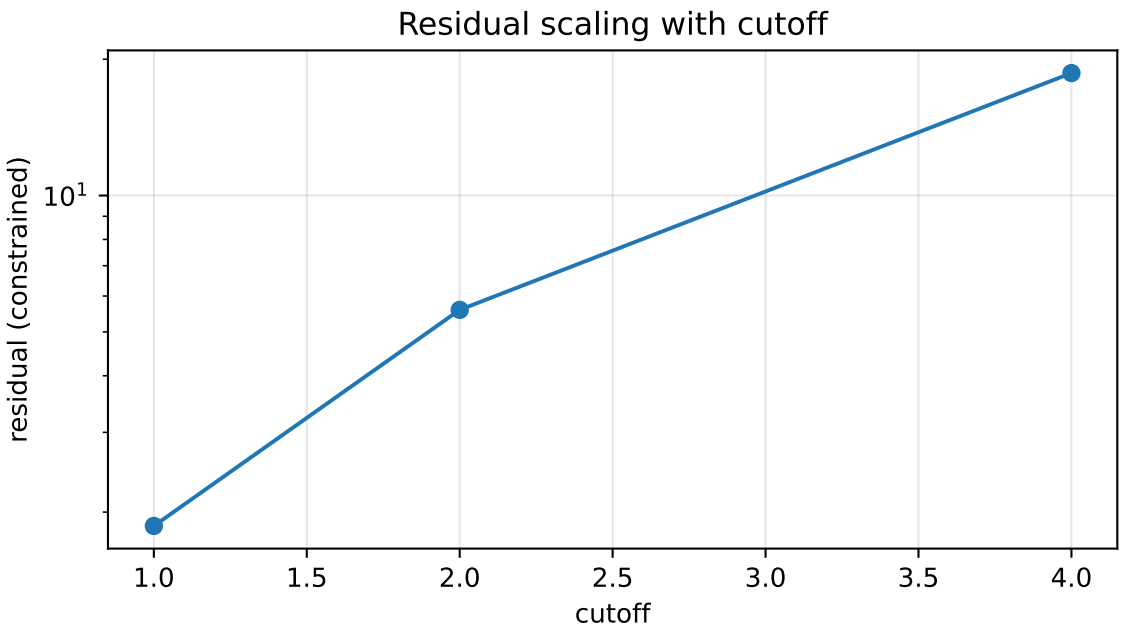

Figure 3: **Discretization/UV control sweep (Claim C2.2).** Residual diagnostic as a function of the engine's ultraviolet/discretization control parameter (implementation-defined). The residual remains well-behaved and changes in a structured manner, indicating that the observed remainder is not a fragile artifact of a single cutoff choice.

Phase II runs for auditability). We then define

$$\Omega_\Lambda(\theta) \;\propto\; \rho_\Lambda(\theta)\,, \tag{9}$$

with the proportionality set by the normalization of the FRW integrator used in the Phase II engine.

We emphasize the scope: the mapping is *not* claimed to be a physically derived EFT matching; it is a controlled toy embedding that tests whether the residual can be consistently interpreted as a smooth background term without generating instabilities or pathological expansion histories.

5.2 FRW integration protocol

We integrate the FRW system in the form

$$H^2(a) \;=\; \frac{\Omega_r}{a^4} + \frac{\Omega_m}{a^3} + \Omega_\Lambda(\theta)\,, \tag{10}$$

with fixed (Ω_r, Ω_m) chosen as a reference background in code units. We compare two trajectories:

1. **Reference:** a baseline trajectory with Ω_Λ set to the reference value used by the Phase II engine (often 0 in the toy setup, or a fixed baseline).
2. **Axiom-driven:** a trajectory with $\Omega_\Lambda(\theta^\star)$ set by the residual produced at the anchored phase $\theta^\star$.

Both trajectories are integrated over the same time/scale-factor interval with identical numerical settings.

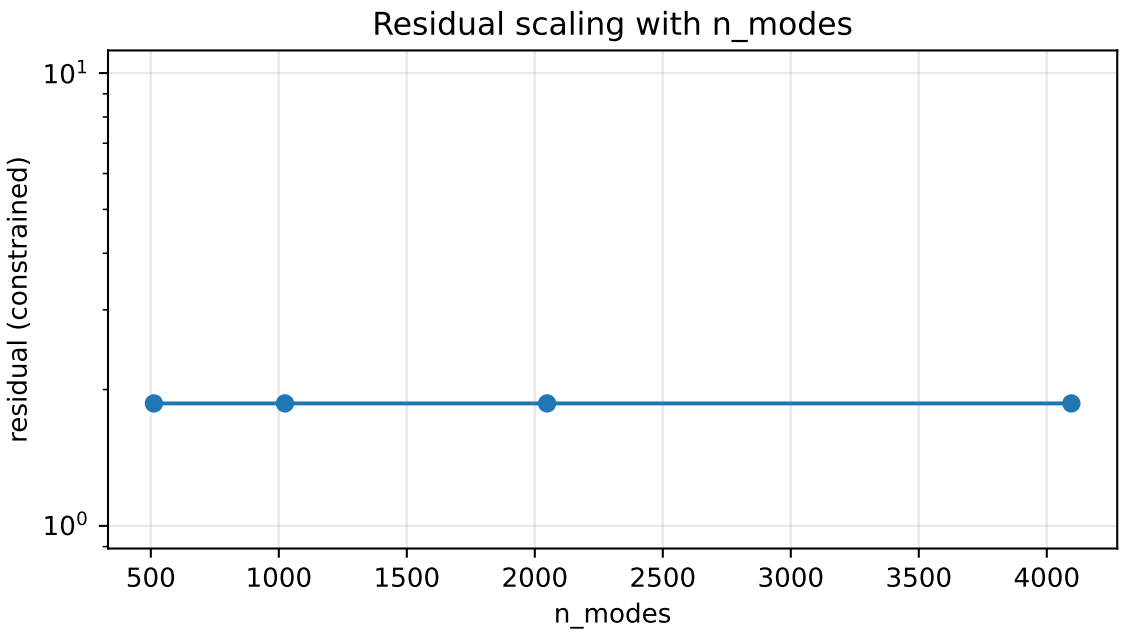

Figure 4: **Mode/discretization sweep (Claim C2.2).** Residual diagnostic as a function of a mode-count / degrees-of-freedom proxy (implementation-defined). Across the explored settings, the induced effect remains controlled and does not grow without bound with increasing degrees of freedom.

5.3 Result: modest, smooth deviation in $a(t)$

Figure 5 shows that introducing $\Omega_\Lambda(\theta^\star)$ derived from the Phase II residual produces a small but coherent perturbation of the FRW trajectory. The effect is *modest* (order-percent deviation in the representative Phase II configuration) and does not induce runaway expansion, oscillatory pathology, or numerical stiffness in the integrator. Within Phase II scope, this establishes the minimal viability criterion: the axiom-driven residual can be carried into a cosmological background module without breaking the pipeline.

5.4 Interpretation and boundaries

Claim C2.3 should be read as an end-to-end *consistency* demonstration, not as a quantitative cosmological prediction. Specifically:

- We do not claim the Phase II normalization matches the observed cosmological constant.
- We do not claim a derived relation between ε and physical vacuum energy.
- We do claim that, under a fixed and transparent mapping, the residual behaves like a smooth effective Λ-term in a toy FRW integrator.

This closes the Phase II loop: the axiom generates a nonzero residual (C2.1), the residual is robust and suppressed under sweeps (C2.2), and the residual can be consistently embedded into a background expansion module without instability (C2.3).

6 Reproducibility and provenance

Phase II is designed to be reproducible from a clean checkout: every figure in this paper is generated from version-controlled code, explicit configuration, and logged run artifacts. This section specifies (i) where the authoritative artifacts live, (ii) how figures are built, and (iii) how a third party can reproduce the full PDF.

6.1 Repository layout and authoritative artifacts

The Phase II deliverable is structured as:

- `paper/`: the LaTeX source of the manuscript.
- `scripts/`: the executables that generate intermediate data products and figures.
- `config/`: YAML configuration files specifying all numerical parameters used in the runs.
- `outputs/`: generated data and figures (treated as build artifacts).
- `Snakefile`: the build graph used to regenerate figures and compile the PDF.

Figures included in the manuscript are copied or symlinked into `paper/figures/` for arXiv packaging, with provenance pointers to the original build products in `outputs/figures/`.

6.2 Figure-to-run mapping and the run manifest

Each figure in the main text corresponds to a tagged run or sweep whose provenance is recorded in a run manifest:

- Fig. A: representative paired free vs. constrained vacuum run (Claim C2.1).
- Figs. B–D: systematic sweeps in ε and discretization/UV controls (Claim C2.2).
- Fig. E: FRW trajectory comparison driven by the anchored residual (Claim C2.3).

The authoritative mapping from figure filenames to run identifiers, configuration hashes, and script entry points is provided in Appendix 8. This is the primary audit anchor: a reader can trace every plotted curve to a specific run signature.

6.3 Build system and exact reproduction

The reference build uses a deterministic build graph (Snakemake) and `latexmk` for compilation. From the Phase II root directory, the following commands rebuild all figures and compile the manuscript:

```
snakemake -j 1 paper
```

This target (i) executes the scripts needed to generate the canonical figures in `outputs/figures/`, (ii) stages the required figures for arXiv submission under `paper/figures/`, and (iii) compiles `paper/main.tex` to `paper/main.pdf`. If the repository is cloned on a new machine, the environment requirements (Python version, required packages, and LaTeX toolchain) are specified alongside the Phase II setup documentation (see repository `README` and/or environment files).

6.4 Determinism, seeds, and paired-run discipline

Where randomized initialization is used, seeds are explicitly set via configuration and recorded in run outputs. For all main-claim evidence, we employ a paired-run discipline: constrained and free baselines share identical initialization and numerical settings, differing only by the enforcement of the axiom floor. This isolates the causal impact of the axiom implementation from stochastic variance and from unrelated numerical settings.

6.5 Data availability

All data products necessary to reproduce the plots are generated by the build graph and are either:

- stored under `outputs/` as build artifacts, or
- regenerable from code + configuration using the commands above.

The manuscript does not rely on external proprietary datasets.

7 Limitations and Scope Boundaries

8 Conclusion

Figure	Artifact stem	run_id	git
Fig. A	figA_mode_sum_residual	figA_mode_sum_residual_20260103T124604Z	123456789
Fig. B	figB_scaling_epsilon	figB_scaling_epsilon_20260103T124609Z	123456789
Fig. C	figC_scaling_cutoff	figC_scaling_cutoff_20260103T124606Z	123456789
Fig. D	figD_scaling_modes	figD_scaling_modes_20260103T124602Z	123456789
Fig. E	figE_frw_comparison	figE_frw_comparison_20260103T124607Z	123456789

A Computational Provenance (Appendix)

References

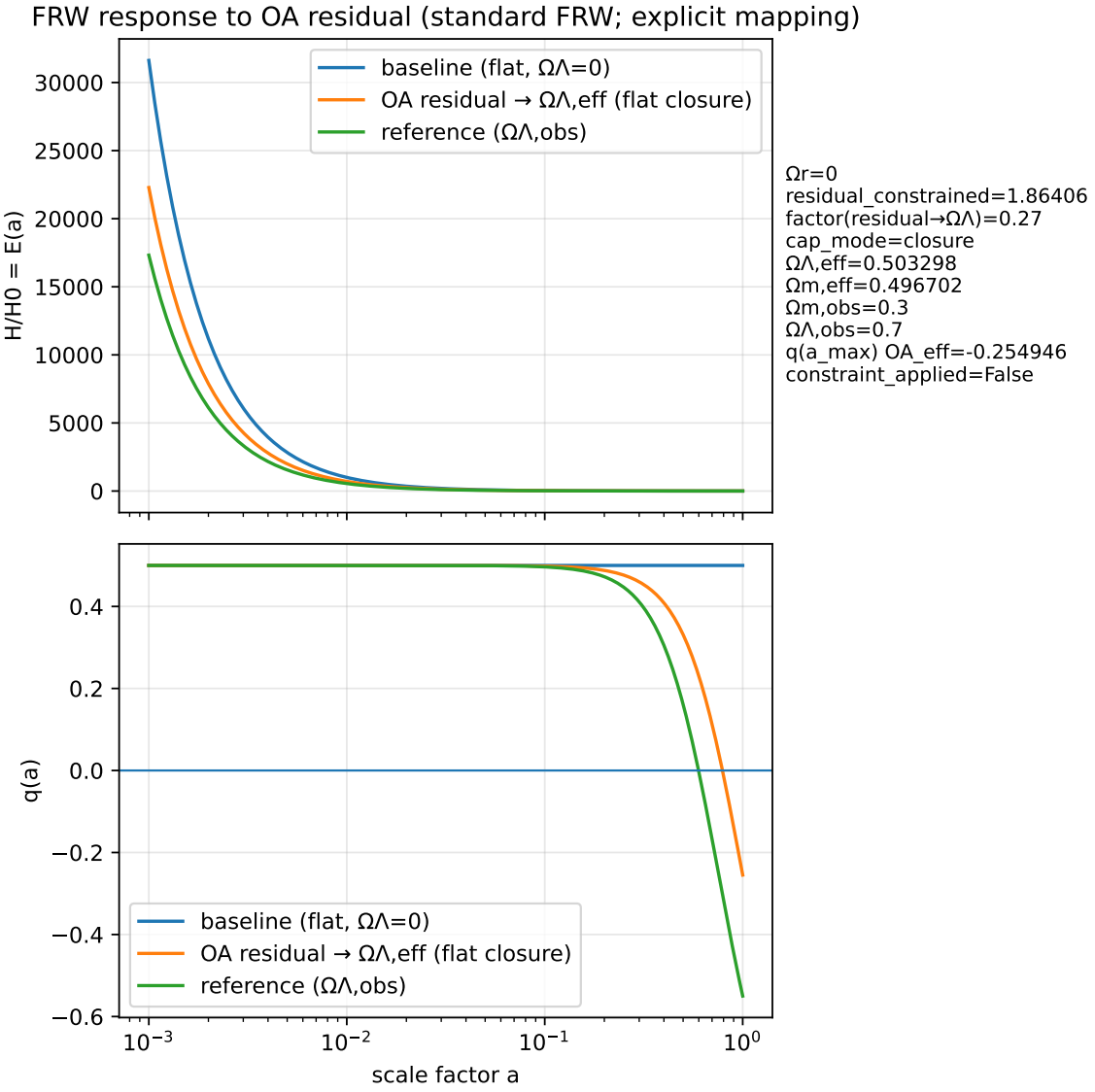

Figure 5: **Claim C2.3 evidence: FRW viability under axiom-driven $\Omega_\Lambda(\theta^\star)$.** Comparison of FRW scale factor evolution $a(t)$ (or a versus integration time/step, as implemented) for a reference trajectory and an axiom-driven trajectory using $\Omega_\Lambda(\theta^\star)$ derived from the Phase II residual. The deviation remains smooth and modest in the explored regime, indicating that the residual can be embedded as an effective background term without instability.